A Low-Power Optical Receiver for Contact-free Programming and 3D Localization of Autonomous Microsystems

Brad Wheeler
Department of Electrical Engineering and Computer Sciences
University of California, Berkeley
Berkeley, California USA
Email: brad.wheeler@berkeley.edu

Andrew Ng
Department of Electrical Engineering and Computer Sciences
University of California, Berkeley
Berkeley, California USA
Email: ang616@berkeley.edu

Brian Kilberg
Department of Electrical Engineering and Computer Sciences
University of California, Berkeley
Berkeley, California USA
Email: bkilberg@berkeley.edu

Filip Maksimovic
Department of Electrical Engineering and Computer Sciences
University of California, Berkeley
Berkeley, California USA
Email: fil@berkeley.edu

Kristofer S. J. Pister
Department of Electrical Engineering and Computer Sciences
University of California, Berkeley
Berkeley, California USA
Email: ksjp@berkeley.edu

***Abstract*—Optical receivers for autonomous microsystems provide benefits such as enabling contact-free optical programming and low-power 3D optical localization. A small, low power optical receiver is presented for transferring program data to a microcontroller's SRAM and detecting optical pulses from a lighthouse localization system. An integrated photodiode is combined with an inverter-based amplifier design to generate a digital waveform from optical input. A pulse width modulation scheme is used to allow clock and data recovery (CDR) to operate without any on-chip clock source. The receiver is able to achieve a data rate of 320 kbps for active and standby powers of 1.52 μW and 640 nW, respectively, while occupying 16,900 μm^2. This optical receiver can also operate as a lighthouse localization receiver, enabling a completely integrated, low power method of localization for a monolithic integrated system. The successful programming of a lighthouse localization routine onto a monolithic integrated system is demonstrated. Using a commercially available HTC Vive V1 lighthouse base station, this optical receiver was able to provide relative azimuth and elevation data with RMS error of 0.386 degrees and 0.312 degrees, respectively, while consuming only 1 mW of power.**

***Index Terms*—localization, optical receiver, microsystems, microrobots, virtual reality, wireless sensor networks, motion capture**

I. Introduction

Integrated systems such as [1], [2] require a way to transfer configuration and program data to on-board memory. Wired programmers are inconvenient and become less practical as systems scale down in size to monolithic proportions. Radio based bootloaders provide a wireless solution, but at the expense of significant power. The addition of an integrated optical receiver requires much less power than an RF receiver and consumes little additional die area.

An integrated optical receiver also can act as a sensor for optical localization. Many wireless sensor network applications of miniaturized, low-power, monolithic integrated systems benefit from accurate localization information in order to provide useful data. Lighthouse localization, a form of optical localization, is suitable for implementation on miniaturized, monolithic integrated systems [3]. An integrated optical receiver can enable both low-power programming and accurate localization in highly-miniaturized monolithic integrated systems.

II. System Design

The Single Chip μMote (SCμM) was designed for micro robot control and miniature wireless sensor network applications. It includes a Cortex M0 processor with 64 kB each of program and data memory, and a 2.4 GHz 802.15.4 and BLE compatible transceiver in a 3x2x0.3 mm^3 chip requiring no external connections except power and ground [2]. The primary goal of the optical receiver was to enable wireless programming of SCμM on the order of 1 s, thus requiring a data rate in the 100s of kbps. The goal was to transfer the majority of the programming burden to an external USB-powered optical programmer in order to reduce the complexity and power required on-chip. A self-clocked approach to clock and data recovery (CDR) was used to eliminate the requirement for a receiver clock which simplifies the receiver and allows more of the power budget to be spent in the front-end amplifier. The receiver is required to work from a default configuration at cold start with no trim and to provide some

978-1-7281-3885-5/19/$31.00 ©2019 IEEE

Authorized licensed use limited to: Univ of Calif Berkeley. Downloaded on June 27,2020 at 01:19:59 UTC from IEEE Xplore. Restrictions apply.

rejection to DC offsets in bright lighting conditions. Optical programming for this design is only required to be done under normally varying lab conditions near room temperature.

The digital output from the optical receiver can be used in several ways. Initially, when 1.5V is applied between power and ground, the chip will boot from ROM and wait for input from the optical bootloader. If the 32 bit start symbol is received, the system executes a hard reset then fills the program memory with the next 64 kB received from the optical receiver. Several other configurations can be accessed from software, including triggering an interrupt on any 32 bit data received, and triggering an interrupt for a particular 32 bit data word. With an external wire, an interrupt can be triggered any time a single optical rising edge is detected. This last option enables sub-microsecond timing of the lighthouse localization signals described in the next section.

III. Lighthouse Localization

Lighthouse localization was initially conceived for localizing smart dust [3]. More recently, it has become a successful and accurate 3D localization technology used in virtual reality and industrial metrology, providing millimeter-scale accuracy [3], [4], [5], [6]. This technology relies on a "lighthouse beacon" that generates a series of wide-angle infrared pulses and precise planar laser scans. These pulses and scans are detected by the localizing motes and their timings are used by the motes to calculate their azimuth and elevation relative to the lighthouse beacon (Figure 1). Lighthouse localization provides unique advantages for localizing large numbers of miniaturized, low power, wireless motes. First, this method scales well computationally with large numbers of motes, because the localization time is independent of the number of motes being localized. Second, the distributed localization computation required by the motes to self-localize is very cheap, which is highly suitable for a miniature low-power microcontroller. Finally, the motes don't require RF communication in order to localize themselves, which frees radio bandwidth for other uses. When coupled with miniaturized monolithic integrated systems, lighthouse localization could enable of host of applications such as fine granularity wireless sensing, body-area networks, and multi-agent control and localization of microrobots.

IV. Clock and Data Recovery

The self-clocked CDR shown in Figure 2 is based on [7] where a pulse width modulation scheme is used to implement an optical wake-up receiver. In this scheme short and long pulses are time delayed and then used as clock edges to sample the incoming pulse stream. The time delay in [7] is implemented by sampling the incoming data stream with a clock running at less than 1 kHz and then delaying for an integer number of clock cycles. The use of such a low clock frequency reduces power consumption but limits data rate to below 100 bps which is insufficient for this application. Instead of increasing the frequency, this work avoids an on-chip clock for sampling by implementing a self-clocking strategy based

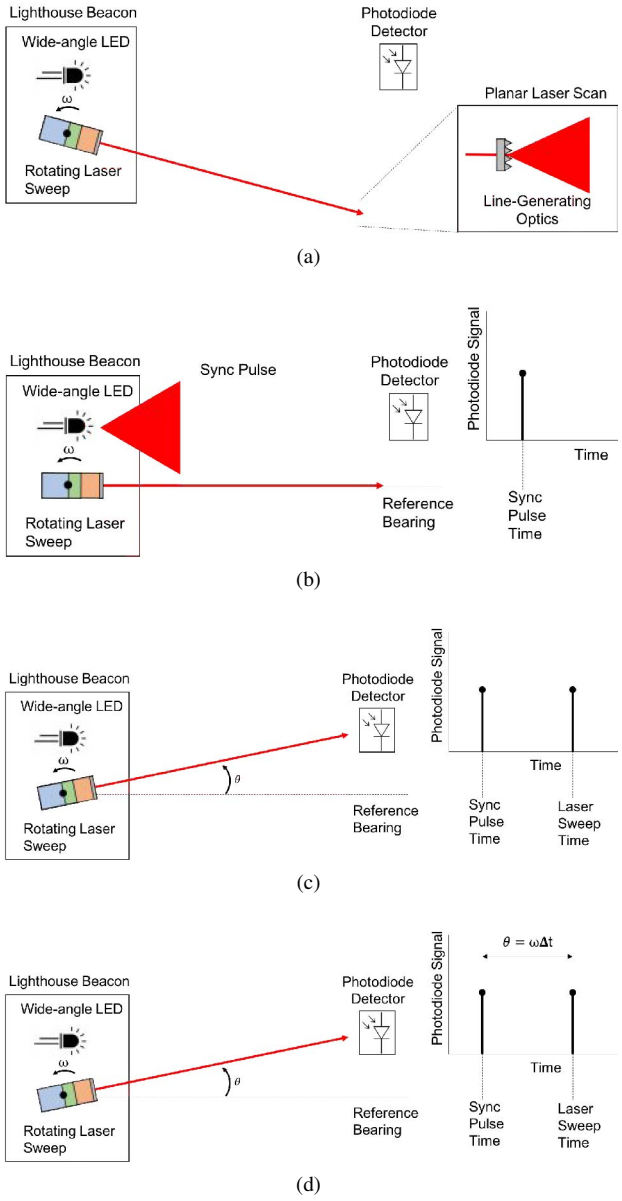

Fig. 1. Illustration of lighthouse localization as implemented in the HTC Vive V1. a.) The system consists of a lighthouse beacon containing a wide-angle LED array, two sets of rotating planar lasers, and a photodetecting system. b.) As the the rotating laser scan passes a reference heading, the LED array flashes and generates a synchronization pulse, which is detected by the photodetector. c.) Once the planar laser scan reaches the photodetector, the photodetector detects the scan and measures the time difference between the sync pulse and the laser scan. d.) Using the constant rotation frequency of the laser scan and the time difference, the photodetector can calculate its heading relative to the reference heading of the lighthouse beacon.

Authorized licensed use limited to: Univ of Calif Berkeley. Downloaded on June 27,2020 at 01:19:59 UTC from IEEE Xplore. Restrictions apply.

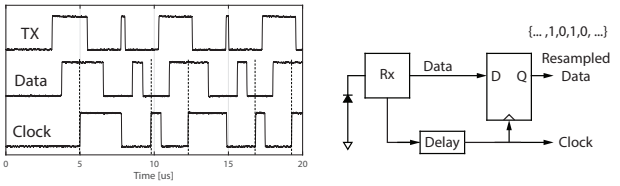

Fig. 2. Block diagram and measured transient waveforms for the RX frontend and self-clocked data recovery.

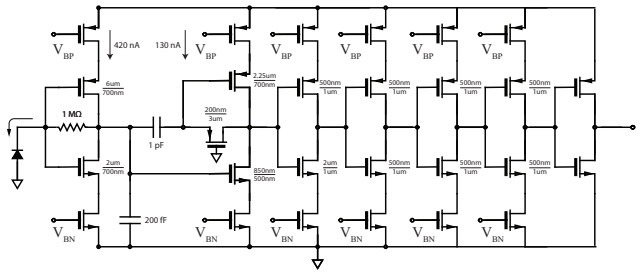

Fig. 3. Schematic of front-end TIA, bandpass filter, and biased inverters.

on an analog delay. The pulse stream coming from the RX front-end is passed through a delay cell built from a chain of current-starved inverters and then combined with a single flip-flop to form the complete CDR.

V. Circuit Design

A. Diode

The front-end uses a deep N-well to substrate diode with an area of 2510 μm^2. The diode was measured to have a responsivity of 0.21 A/W to IR light at 850 nm. The diode is held at a reverse bias of $V_{DD}/2$ by the self biased inverter transimpedance amplifier (TIA). The simulated junction capacitance at this bias was 2.26 pF which agrees within 10% of the measured value for this junction type of 1 fF/μm^2. The external optical programmer used in this system is based on a SFH4555 IR emitter with irradiance of 550 mW/sr and has a target range of less than 10 cm.

B. Transimpedance Amplifier

A TIA architecture was chosen based on [8] and was designed using a self-biased inverter for its simplicity and current reuse. The feedback simplifies biasing of the photodiode and allows for higher data rates than a high impedance design as in [7]. The current limiting devices for both the amplifier and the analog delay cells are biased using constant g_m circuits. DC offsets from ambient light are reduced by AC coupling the TIA to the second gain stage, which is based on the baseband amplifier design in [9]. The second stage is followed by five inverter gain stages to rectify the incoming signal to digital levels before passing it to the CDR.

C. Delay Cell

The analog delay cell consists of additional current-starved inverters like those in Figure 3. The nominal target delay value t_d is 1 μs to enable data rates in the 100s of kbps. Only one corner of devices was received from fabrication so measurement results are unavailable for process variation, but simulations indicate that the process-dependent shift in t_d tracks the shift in pulse widths, minimizing the affect on the CDR.

VI. Digital Backend

The recovered clock and data bit stream is routed to a digital block which provides the programming interface to the microprocessor. This block performs three main functions: 1) Search for a start sequence which indicates that the digital system should execute a hard reset to prepare for bootloading 2) Perform 4B/5B decoding on the incoming data stream to recover the original program data and 3) Convert the serial bit stream to a format equivalent with the pre-existing three-wire programming bus which loads program data into instruction memory. A CRC value is calculated by the programmer and inserted into the payload so the the microprocessor can check the validity of the program data at the start of execution.

The 4B/5B coding step is used to DC balance the incoming data stream to avoid transient issues caused by the AC coupling in the receiver settling to data-dependent values. Compiled program binaries often have long strings of unchanging bits which cause changes in the pulse width outputs of the frontend as shown in Figure 4. If left uncorrected this pulse expansion will cause incorrect reception of long strings of zero bits as the pulse width will expand beyond the delay value and begin registering as ones instead of zeros.

Programming also provides an opportunity to calibrate the initial frequencies of the various free-running clocks on the mote. The optical programmer is based on a microcontroller with a crystal-based time reference and thus it transmits data at an accurate rate. The programmer can continue sending data after programming has completed in order for the mote to measure and calibrate its own clocks against this known data rate. This provides the mote with an initial frequency calibration that can then be updated by other mechanisms as discussed in [2] and [10].

VII. Measurement Results

The proposed receiver was fabricated in TSMC 65LP and the die photo is shown in Figure 5. The total design including the photodiode, amplifiers, delay cell, and CDR occupies 16,900 μm^2. An FPGA-based TDC [11] was used to measure individual pulses' width and delay. The optical programmer was built using an SFH4555 IR emitter LED driven by a micro-controller able to generate pulses with widths controllable in increments of 5.6 ns. Long strings of unchanging data cause shifts in DC bias which lead to changes in pulse width over time. The following measurements use 4B5B encoding to avoid this issue by DC balancing the data stream.

The active power consumption was measured to be 1.52 μW and the standby power was 640 nW. Figure 6(a) is an example histogram obtained via the TDC setup showing the distribution of short and long pulses as well as the delay time. Figure 6(b)

Authorized licensed use limited to: Univ of Calif Berkeley. Downloaded on June 27,2020 at 01:19:59 UTC from IEEE Xplore. Restrictions apply.

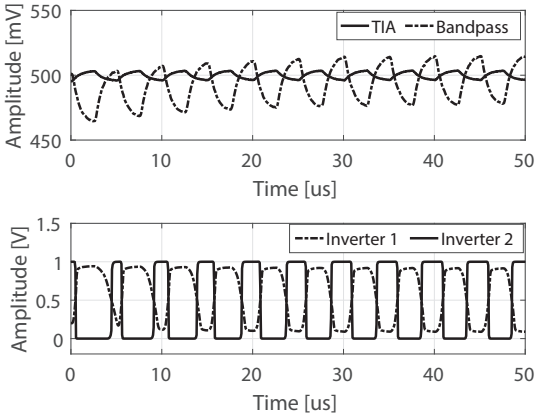

Fig. 4. Transient simulation showing how strings of non-changing data cause DC bias shifts which lead to pulse width expansion.

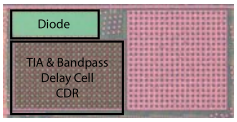

Fig. 5. Die photo of the optical receiver which occupies 16,900 um^2.

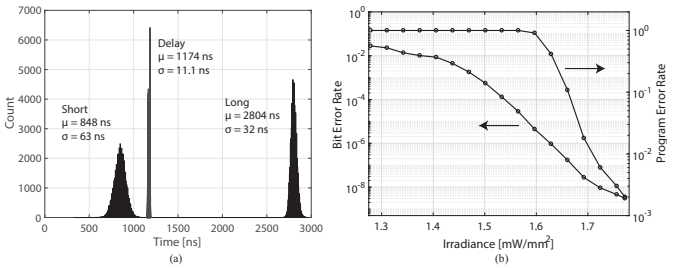

Fig. 6. (a) Histogram showing measurement results for short and long pulses and delay time. (b) BER and PER vs irradiance for 64 kB 4B5B payloads.

shows the measured Bit Error Rate and Program Error Rate (PER defined as the occurrence of a single bit error in a 64 kB payload) for a given input irradiance. An irradiance of 1.7 $\mathrm{mW/mm^2}$ is sufficient to ensure fewer than one payload bit error per one hundred programming cycles.

A. Supply Voltage

The receiver is designed to operate at a nominal supply voltage of 0.8 V, which is a regulated voltage generated on-chip. The effect of varying supply voltage on pulse widths and delays is shown in Figure 7(a). Error bars indicate the maximum and minimum values recorded during a 4 kB 4B5B encoded payload. The slope of the change in delay time is 125 ns/V which is insignificant when compared to the variation in pulse widths from the TIA. Further excursions away from nominal supply point can be tolerated by adjusting the pulse widths from the transmitter.

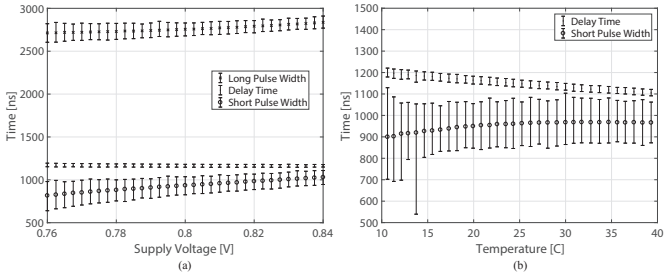

Fig. 7. Pulse and delay variation due to (a) supply voltage and (b) temperature

B. Temperature

Figure 7(b) shows the variation of the short pulse widths and delay times across temperature. Again the variation of the pulse widths from the TIA are the limiting factor and will cause zeros to get clocked as ones at elevated temperatures when the width of the short pulse exceeds the delay time. The slope of the delay variation with temperature is 3.4 ns/°C.

VIII. Lighthouse Localization Experiments

A. Experimental Setup

To conduct localization experiments, the mote was optically programmed with software that continuously monitored the optical receiver output for rising and falling edges. The pulse width between these edge events was time-stamped using an on-chip free-running 10 MHz RC oscillator. This oscillator can be tuned to within an accuracy of ± 1500 ppm by comparing its frequency to the known data rate of the optical programmer. The width of the received pulses served as input to a finite state machine that searched for valid sequences of lighthouse pulses. A valid set of pulse measurements consists of an azimuth sync pulse, an azimuth laser sweep pulse, an elevation sync pulse, and an elevation laser sweep pulse. When a proper sequence of those four pulses was found the mote would print the time-stamp values corresponding to the rising edges of these four pulses. The difference between sync and laser sweep time-stamps can then be used to calculate azimuth and elevation relative to the lighthouse base station. Any pulse measurements that did not match this four-pulse lighthouse sequence were discarded.

The experiment was designed to test the tracking performance of the optical receiver when using a commercial-off-the-shelf HTC Vive V1 lighthouse. The optical receiver chip was moved through a trajectory while tracking itself using the IR pulses and sweeps from the lighthouse beacon. The ground truth of the receiver's trajectory was obtained using an Optitrack motion capture system. This system was synchronized to the sync pulse of the lighthouse beacon to avoid infrared interference. The experimental setup is illustrated in Figure 8, which shows the ground truth trajectory of the receiver in relation to the position and orientation of the lighthouse beacon. Only one lighthouse beacon was used, so the optical receiver system was calculating its azimuth and elevation relative to the lighthouse beacon, not its full 3D location

Authorized licensed use limited to: Univ of Calif Berkeley. Downloaded on June 27,2020 at 01:19:59 UTC from IEEE Xplore. Restrictions apply.

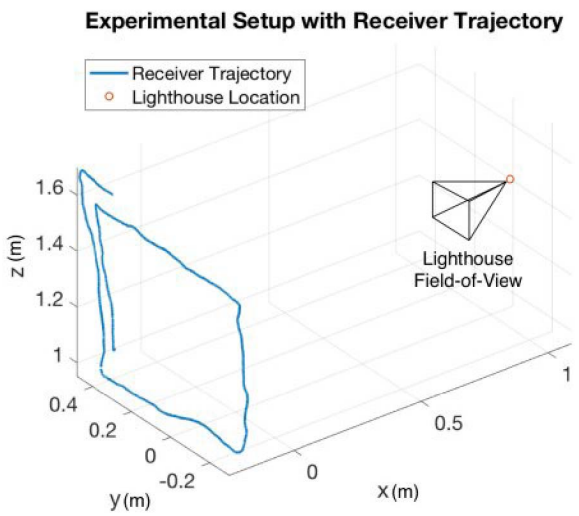

Fig. 8. Illustration of lighthouse experimental setup. The blue line indicates the ground truth 3D trajectory of the optical receiver, obtained by motion capture. The red dot indicates the location of the lighthouse beacon, and the field-of-view indicates the direction the lighthouse beacon is pointing.

which would require two lighthouse beacons to calculate. The azimuth and elevation of the receiver in this experiment are approximately proportional to the y and z coordinates of the receiver, respectively. The receiver was approximately 1.3 meters away from the lighthouse throughout the experiment.

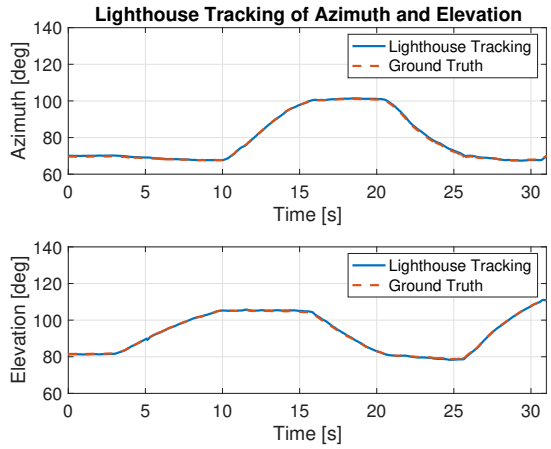

Fig. 9. Azimuth and elevation tracking of optical receiver, compared to ground truth. The RMS error of azimuth tracking was 0.386 degrees. Elevation tracking's RMS error was 0.312 degrees.

B. Experimental Results

The measured azimuth and angle trajectory are compared in Figures 9 and 10. Note that the azimuth and elevation of the receiver is approximately proportional to its trajectory projected onto the $(-y, z)$ plane. A post-hoc calibration to take into account discrepancies in lighthouse position and alignment relative to ground truth was applied to the data.

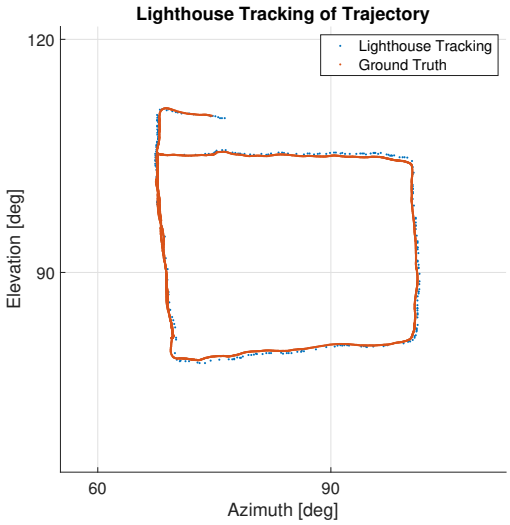

Fig. 10. Performance of azimuth and elevation tracked by the optical receiver compared to the ground truth trajectory.

This consisted of a lighthouse azimuth alignment adjustment of 2.5 degrees, a lighthouse elevation alignment adjustment of 0.5 degrees, and a lighthouse centroid adjustment of 5 cm. A simple filtering algorithm was used to reject outlying measurements. This algorithm rejected measurements that were more than 5 degrees different than the previous measurement. The RMS error of the azimuth measurements was 0.386 degrees, which would correspond to a 9 mm error at a distance of 1.3 m. The RMS error of the elevation measurements was 0.312 degrees which corresponds to a 7 mm error at a distance of 1.3 m.

IX. Discussion

The preceding experiment demonstrated the full functionality of the optical receiver: touchless optical programming of a monolithic microprocessor system and optical self-localization based on lighthouse beacon pulses and sweeps. Other than a 1.5V power source supplied via two bond pads, there were no external components required on the mote side of this demonstration. The on-chip transceiver was not used to report position in this experiment, but that capability is available. This functionality is useful for miniaturized, low-power, and ubiquitous microsystems. Optical programming decreases the amount of power required for programming and eliminates the need for bulky wired connections for programming, which is beneficial for miniature integrated systems. The ability to receive lighthouse localization pulses with the integrated optical receiver will enable accurate localization of large numbers of miniaturized integrated microsystems. Indeed, the entire integrated system used in the preceding localization experiment was only 2x3x0.3 mm^3 (without power supply) and its measured power consumption during localization was only 1 mW. For example, this localization ability could be used by microrobots such as postage-stamp sized ionocraft, mm-scale hexapods, and jumping microrobots [12], [13], [14].

Authorized licensed use limited to: Univ of Calif Berkeley. Downloaded on June 27,2020 at 01:19:59 UTC from IEEE Xplore. Restrictions apply.

X. Conclusion

Contact-free programming and accurate localization are beneficial for autonomous microsystems. In order to enable contact-free programming, a low power optical receiver was developed. A self-clocked CDR circuit was utilized to remove the need for any on-chip clock source. Receiver power, area, and complexity were reduced by simplifying the clock recovery circuit and utilizing inverter based amplifiers and delay cells. This receiver was demonstrated transferring program data to an SoC platform at data rates of 100s of kbps, which will enable convenient contact-free programming of microsystems.

This receiver was also successfully used to program a SCμM chip and operate as a lighthouse localization receiver, providing localization accuracy of roughly 0.3 degrees for azimuth and 0.4 degrees for elevation angles relative to an HTC Vive lighthouse base station. This result could pave the way for accurate localization of miniaturized systems such as microrobots and wireless sensor networks. Future work will focus on using this optical receiver to localize autonomous microrobots and wireless body sensor networks.

References

[1] Y. Lee, S. Bang, I. Lee, Y. Kim, G. Kim, M. H. Ghaed, P. Pannuto, P. Dutta, D. Sylvester, and D. Blaauw, "A modular 1 mm^3 die-stacked sensing platform with low power i^2c inter-die communication and multi-modal energy harvesting," *IEEE Journal of Solid-State Circuits*, vol. 48, no. 1, pp. 229–243, Jan 2013.

[2] F. Maksimovic, B. Wheeler, D. C. Burnett, O. Khan, S. Mesri, I. Suciu, L. Lee, A. Moreno, A. Sundararajan, B. Zhou *et al.*, "A crystal-free single-chip micro mote with integrated 802.15. 4 compatible transceiver, sub-mw ble compatible beacon transmitter, and cortex m0," in *2019 Symposium on VLSI Circuits*. IEEE, 2019, pp. C88–C89.

[3] K. Römer, "The lighthouse location system for smart dust," in *Proceedings of the 1st international conference on Mobile systems, applications and services*. ACM, 2003, pp. 15–30.

[4] N. Metrology, "ispace: Large volume metrology, tracking, and positioning," Brochure, 2010. [Online]. Available: "https://www.nikonmetrology.com/en-gb/product/igps", last accessed on 8/1/2019

[5] H. Vive, "Vive vr system," Webpage, 2019. [Online]. Available: "https://www.vive.com/us/product/vive-virtual-reality-system/", last accessed on 8/1/2019

[6] M. Borges, A. Symington, B. Coltin, T. Smith, and R. Ventura, "Htc vive: Analysis and accuracy improvement," in *2018 IEEE/RSJ International Conference on Intelligent Robots and Systems (IROS)*. IEEE, 2018, pp. 2610–2615.

[7] G. Kim, Y. Lee, S. Bang, I. Lee, Y. Kim, D. Sylvester, and D. Blaauw, "A 695 pw standby power optical wake-up receiver for wireless sensor nodes," in *Custom Integrated Circuits Conference (CICC), 2012 IEEE*. IEEE, 2012, pp. 1–4.

[8] B. S. Leibowitz, B. E. Boser, and K. S. Pister, "Cmos smart pixel for free-space optical communication," in *Sensors and Camera Systems for Scientific, Industrial, and Digital Photography Applications II*, vol. 4306. International Society for Optics and Photonics, 2001, pp. 308–319.

[9] B. W. Cook, A. Berny, A. Molnar, S. Lanzisera, and K. S. Pister, "Low-power 2.4-ghz transceiver with passive rx front-end and 400-mv supply," *IEEE Journal of Solid-State Circuits*, vol. 41, no. 12, pp. 2757–2766, 2006.

[10] I. Suciu, F. Maksimovic, D. Burnett, O. Khan, B. Wheeler, A. Sundararajan, T. Watteyne, X. Vilajosana, and K. Pister, "Experimental Clock Calibration on a Crystal-Free Mote-on-a-Chip," in *CNERT: Computer and Networking Experimental Research using Testbeds*, 2019.

[11] T. Xiang, L. Zhao, X. Jin, T. Wang, S. Chu, C. Ma, S. Liu, and Q. An, "A 56-ps multi-phase clock time-to-digital convertor based on artix-7 fpga," in *Real Time Conference (RT), 2014 19th IEEE-NPSS*. IEEE, 2014, pp. 1–4.

[12] D. S. Drew, N. O. Lambert, C. B. Schindler, and K. S. J. Pister, "Toward controlled flight of the ionocraft: A flying microrobot using electrohydrodynamic thrust with onboard sensing and no moving parts," *IEEE Robotics and Automation Letters*, vol. 3, no. 4, pp. 2807–2813, Oct 2018.

[13] D. S. Contreras and K. S. Pister, "A six-legged mems silicon robot using multichip assembly," in *Hilton Head Workshop*, 2018.

[14] H. C. G. K. S. J. P. C. B. Schindler, J. T. Greenspun, "A jumping silicon microrobot with electrostatic inchworm motors and energy storing substrate springs,," in *2019 20th International Conference on Solid-State Sensors, Actuators and Microsystems (TRANSDUCERS)*, June 2017.

Authorized licensed use limited to: Univ of Calif Berkeley. Downloaded on June 27,2020 at 01:19:59 UTC from IEEE Xplore. Restrictions apply.